

## Design of driver assistance system for air cushion vehicle with uncertainty based on model knowledge neural network

Mingyu Fu, Shuang Gao\*, Chenglong Wang, Mingyang Li

*College of Automation, Harbin Engineering University, Harbin, 150001, China*



### ARTICLE INFO

**Keywords:**

Motion control  
Air cushion vehicle  
Uncertainty  
Neural network  
Adaptive control

### ABSTRACT

In this paper, considering the difficult maneuverability of the air cushion vehicle (ACV), a driver assistance system (DAS) of ACV including an intuitive human-computer interface, DAS monitor and DAS controller is developed for humans. The human-computer interface is easy to be understood and used for humans. And as DAS monitor, appropriate sensors installed at handles of rudders and propellers are used to monitor driver's operational changes. For the design of DAS controller, model knowledge neural network (MKNN) method is first proposed in this paper to deal with the parameter uncertainty of ACV's complex model. Then the MKNN-based controller is designed as the DAS controller. The DAS with MKNN-based controller can assist drivers in better control operations according to their action instructions. And numerical simulations are implemented to demonstrate the effectiveness and superiority of the developed DAS with MKNN-based controller.

### 1. Introduction

Air cushion vehicle (ACV) as shown in Fig. 1 has a flexible skirt system around its periphery to seal the cushion air (Yun and Bliault, 2000). It can be lifted up by a large enough air cushion force to get amphibious performance and run at a high speed. Thus ACV has been the focus of many oceanic research works including the exploration of oceans, transportation, scientific and military missions, and more (Fu et al., 2017, 2018).

The ACV has very little contact with the water surface and the low righting moments at small ranges of an ACV hovering over water result in rolling, pitching, yawing, drifting and surging motions all being significant (Yun and Bliault, 2000). A maneuvering hovercraft moves with an angle of drift and generates an asymmetric wave pattern leading to the appearance of two additional reactions, the side force and yawing moment (Zilman, 2006). If the drift angle exceeds the angle of drift which corresponds to the maximum of hydrodynamic forces, the behavior of ACV will be nonstable (Zilman, 1993). And when the ACV is turning, roll motion always exists and increases with the increase of the turn rate and drift angle (Tao and Chengjie, 2012). For safety, a higher operating requirement for drivers is needed in the high-speed moving process to prevent dangers like stern-kickoff, plough-in, great heeling and etc. (Fu et al., 2018; Zilman, 1993; Hua, 2008). To lighten this burden, the study about driving control of ACV is meaningful.

However, from a detailed review of the available literature about

the driving control of ACV (Sira-Ramirez, 2002; Zhao and Pang, 2010; Morales et al., 2015; Rigatos and Raffo, 2015; Shojaei, 2015), only simple three degrees of freedom (DOF) model were adopted. And aerodynamic and hydrodynamic forces and moments acting on the body were not represented in their equations of motion. It's worth noting that four DOF model including roll motion is closer to the performance of the real ship than three DOF model for the study of ACV's motion control (Fu et al., 2018; Jun and Huang, 2007). Any analysis of a marine vehicle must include the analysis of the structure of these forces and moments. Formally, after years of efforts by researchers (Cohen et al., 2001; Dyachenko, 1999; Doctors, 1997; Doctors and Sharma, 1972; Newman and Poole, 1962; Okita et al., 2001; Sahin and Hyman, 2001; Tuck and Lazauskas, 2001; Tuck et al., 2002), drags of ACV can be computed by using essentially the same formulas. But they are affected by unavoidable uncertainties in the problem parameters caused by the limitation of test, the error of manual record, the measurement error of instrument, especially other unknown uncertainty like unknown disturbance (Zilman, 2006).

Intelligent controller can learn the dynamics of the robots with uncertainty online, and tune the parameters and structure of the controller according to the operating dynamics and conditions without requiring the mathematical model of the control plant (Lu et al., 2018), such as fuzzy logic systems (Sanchez et al., 2015; Xia et al., 2018; Wang et al., 2017; Chen et al., 2018; Hwang et al., 2014; Lin et al., 2018) and artificial neural networks (Xia and Huo, 2016; Feng and Wen, 2015; Liu

\* Corresponding author.

E-mail address: gaussian@hrbeu.edu.cn (S. Gao).



Fig. 1. 3D model of ACV. Photo is from the international cooperation project of authors.

et al., 2015; Zhang et al., 2015; Mu et al., 2017; Ni et al., 2018). However, the authors believe that the model knowledge obtained by researchers through research and summarization of mathematical models for many years is also valuable and meaningful. The model knowledge that people have mastered over the years should not be abandoned by existing intelligent control method, but be combined with them to get better performance. Hence, model knowledge neural network (MKNN) method which integrates useful ACV's model knowledge into the structure of classical radial basis function neural network is first proposed in this paper. And a MKNN-based controller is designed to deal with the parameter uncertainty.

Moreover, the traditional automatic driving systems are completely controlled by the controller during it is used, and humans cannot intervene unless the automatic driving function is turned off. However, sometimes, what humans expect is to assist them in their operations, rather than giving up their right to operate. So, driver assistance system (DAS) of ACV is designed for humans in this paper. The DAS integrates automatic control and manual operation very well, and can assist the drivers in operating when necessary.

The paper is organized as follows: In section 2, four DOF model of ACV is established. DAS including DAS interface, DAS monitor and DAS controller are described and designed in section 3. Simulations are shown in section 4. Finally, the conclusion of this work is summarized in section 5.

## 2. ACV model description

**Assumption 1.** The motions of pitch and heave are not discussed. The fan flow  $Q$  of cushion fans is assumed to be constant.

**Assumption 2.** The ACV has two same air propellers and two same air rudders, which are symmetrically mounted at the tail of the hull as shown in Fig. 2, and they can only be operated simultaneously, not

separately.

Four DOF model of ACV are as follows:

$$\begin{bmatrix} \dot{x} \\ \dot{y} \\ \dot{\phi} \\ \dot{\psi} \end{bmatrix} = \begin{bmatrix} \cos \psi & -\sin \psi \cos \phi & 0 & 0 \\ \sin \psi & \cos \psi \cos \phi & 0 & 0 \\ 0 & 0 & 1 & 0 \\ 0 & 0 & 0 & \cos \phi \end{bmatrix} \begin{bmatrix} u \\ v \\ p \\ r \end{bmatrix} \quad (1)$$

$$\begin{bmatrix} m\ddot{u} \\ m\ddot{v} \\ J_x\ddot{p} \\ J_z\ddot{r} \end{bmatrix} = \begin{bmatrix} -mvr \\ -muv \\ 0 \\ 0 \end{bmatrix} + \begin{bmatrix} F_{x_D} + 2F_{x_R} + 2F_{x_P} \\ F_{y_D} + 2F_{y_R} \\ M_{x_D} + 2M_{x_R} \\ M_{z_D} + 2M_{z_R} \end{bmatrix} \quad (2)$$

where  $u, v, p, r$  represent the surge, sway, roll and yaw velocities, respectively.  $x$  and  $y$  are the coordinates of the ACV's center of mass in the earth coordinate system,  $\phi, \psi$  are roll and yaw angles, respectively.  $m, J_x$  and  $J_z$  are ACV's mass and moment of inertia respectively.  $F_{x_P}$  is the surge force generated by an air propeller.  $M_{z_R}$  is the yaw moment generated by an air rudder and  $F_{x_R}, F_{y_R}, M_{x_R}$  are its effect on other DOFs.  $[F_{x_D}, F_{y_D}, M_{x_D}, M_{z_D}]^T$  are the total drags written as:

$$\begin{aligned} F_{x_a} &= -0.5\rho_a V_a^2 C_{x_a} S_{PP} \\ F_{y_a} &= -0.5\rho_a V_a^2 C_{y_a} S_{LP} \\ M_{x_a} &= -0.5\rho_a V_a^2 C_{mx_a} S_{PP} l_c + F_{y_a} z_a \\ M_{z_a} &= -0.5\rho_a V_a^2 C_{mz_a} S_{HP} H_{hov} + F_{y_a} x_a + F_{x_a} y_a \\ F_m &= \rho_a V_a Q, \\ F_{wm} &= C_{wm} p_c^2 B_c / \rho_w \\ F_{sk} &= 0.5\rho_w V_a^2 C_{sk} (h/l_{sk})^{-0.34} l_{sk} S_c^{0.5} + (2.8167(p_c/l_c)^{-0.259} - 1) F_{wm} \\ F_c &= 2l_c \varphi p_c (0.5B_c \tan \phi + h_0) \\ M_G &= Gh_m \tan \phi \\ F_{x_D} &= F_{x_a} + F_m \cos \beta + F_{wm} \cos \beta + F_{sk} \cos \beta \\ F_{y_D} &= F_{y_a} + F_m \sin \beta + F_{wm} \sin \beta + F_{sk} \sin \beta + F_c \\ M_{x_D} &= M_{x_a} + F_m z_m \sin \beta + F_{wm} z_{wm} \sin \beta + F_{sk} z_{sk} \sin \beta + Gh_m \tan \phi \\ &\quad + F_c z_c \\ M_{z_D} &= M_{z_a} + F_m x_m \sin \beta + F_m y_m \cos \beta + F_{wm} x_{wm} \sin \beta + F_{wm} y_{wm} \cos \beta \\ &\quad + F_{sk} x_{sk} \sin \beta + F_{sk} y_{sk} \cos \beta + F_c x_c \end{aligned} \quad (3)$$

where  $F_{x_a}, F_{y_a}, M_{x_a}, M_{z_a}$  mean aerodynamic profile drag in four DOF, respectively.  $F_m, F_{wm}, F_{sk}, F_c$  mean air momentum drag, wave-making drag, skirt drag and cushion force, respectively.  $C_{x_a}, C_{y_a}, C_{mx_a}, C_{mz_a}, C_{wm}, C_{sk}$  are the corresponding drag coefficients.  $M_G$  is the restoring moment during rolling.  $l_c$  and  $B_c$  denote cushion length and beam,  $S_{PP}, S_{LP}$  and  $S_{HP}$  are positive, lateral and horizontal projection areas,  $S_c$  means cushion area,  $\beta$  means drift angle,  $p_c$  means cushion pressure,  $h$  is the average clearance for air leakage in static hovering mode,  $h_m$  and  $h_0$  mean metacentric and initial lift height,  $l_{sk}$  is the total peripheral length of the skirts,  $\phi$  is the discharge coefficient,

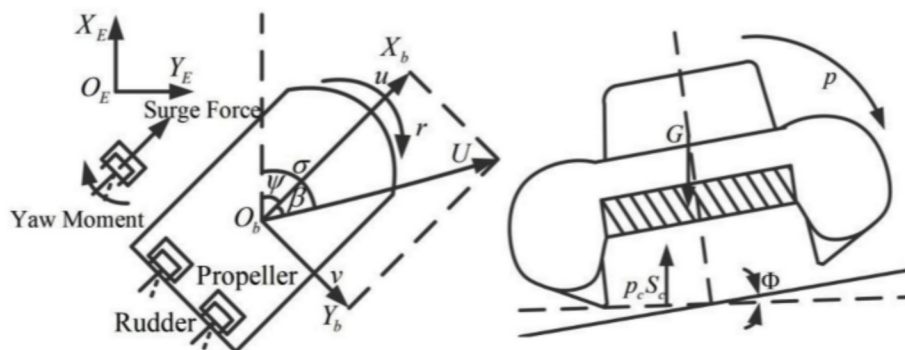


Fig. 2. A brief picture of underactuated ACV.

$H_{hov}$  is the height of ACV,  $\rho_a$  and  $\rho_w$  are air and water density,  $z_a$ ,  $z_m$ ,  $z_{wm}$ ,  $z_{sk}$  and  $z_c$  are the heights of each force's acting point relative to the craft's mass center,  $(x_a, y_a)$ ,  $(x_m, y_m)$ ,  $(x_{wm}, y_{wm})$ ,  $(x_{sk}, y_{sk})$ ,  $(x_c, y_c)$  are the coordinates of these acting points.  $V_a$  can be obtained by

$$\begin{aligned} V_a &= \sqrt{[u + V_w \cos(\beta_w - \psi)]^2 + [v + V_w \sin(\beta_w - \psi)]^2} \\ \beta_a &= \tan^{-1} \left[ \frac{v + V_w \sin(\beta_w - \psi)}{u + V_w \cos(\beta_w - \psi)} \right] \end{aligned} \quad (4)$$

in which  $V_a$  and  $\beta_a$  are relative wind speed and direction,  $V_w$  and  $\beta_w$  are absolute wind speed and direction.

And from (Tao and Chengjie, 2012) and Assumption 2,  $[2F_{x_R}, 2F_{y_R}, 2M_{x_R}, 2M_{z_R}]^T$  can be calculated as follows:

$$\begin{aligned} 2F_{x_R} &= -C_{x_R}\rho_a v_R^2 S_R \\ 2F_{y_R} &= C_{y_R}\rho_a v_R^2 S_R \\ 2M_{x_R} &= -2F_{y_R}z_R \\ 2M_{z_R} &= 2F_{y_R}x_R + F_{x_R}y_{R1} + F_{x_R}y_{R2} \\ &= 2F_{y_R}x_R \end{aligned} \quad (5)$$

where  $(x_R, y_{R1})$  and  $(x_R, y_{R2})$  are the acting point coordinates of rudder forces,  $z_R$  is their height which is relative to the center of gravity plane.  $C_{x_R}$  and  $C_{y_R}$  are rudder force coefficients associated with rudder angle.  $S_R$  is the area of the rudder.  $v_R$  is the inflow velocity of rudder and given by

$$v_R = \begin{cases} V_a \cos \beta_a + \sqrt{F_{x_p}/(\rho_a S_d)} & F_{x_p} \geq 0 \\ V_a \cos \beta_a - \sqrt{|F_{x_p}|/(2\rho_a S_d)} & F_{x_p} < 0 \end{cases} \quad (6)$$

where  $S_d$  is the duct outlet area of air propellers. More details can be found in (Yun and Bliault, 2000; Fu et al., 2017, 2018).

To facilitate the design of the latter controller, we define the following rules:

$$\begin{aligned} \tau_{F_x} &= 2F_{x_p} \\ \tau_{M_z} &= 2M_{z_R} \end{aligned} \quad (7)$$

Then from (5), we have

$$\begin{aligned} F_{x_R} &= -\frac{C_{x_R}}{2C_{y_R}x_R}\tau_{M_z} \\ F_{y_R} &= \frac{1}{2x_R}\tau_{M_z} \\ M_{x_R} &= -\frac{z_R}{2x_R}\tau_{M_z} \end{aligned} \quad (8)$$

### 3. Design of driver assistance system

In this paper, the design of driver assistance systems includes three parts: DAS interface, DAS monitor and DAS controller.

#### 3.1. DAS interface

The human-computer interface of the DAS is shown as Fig. 3. There are four parts in the interface including working mode, monitor, controller and motion display.

Part A: Working mode part displays the current working mode: "Enable" or "Unable" of the DAS.

Part B: Monitor part displays the current driver's action on the handles of rudders and propellers.

Part C: Controller part displays the current states of speed, course and turn rate assistance subsystems and their values.

Part D: Motion display part can intuitively show the motion state of ACV.

#### 3.2. DAS monitor

Selecting the appropriate sensors to install on the handles (as shown in Fig. 4) and monitor the driver's action on the handles: "hold" or "release". These sensors can be pressure transducer, temperature transducer or other suitable sensors.

**Speed assistance subsystem:** During the driver's operation, relative sensors are working to monitor the action of driver on handles of propellers. If the driver releases the handles, it means the driver wishes to remain at the current speed subjectively. In this case, if the speed is still changing, it indicates that there are other reasons for the change of speed. Then, the speed assistance subsystem starts and helps the driver control the speed at the desired value.

**Turn rate assistance subsystem:** During the driver's operation, relative sensors are working to monitor the action of driver on handle of rudders. If the driver releases the handle, it means the driver wishes to remain at the current turn rate subjectively. In this case, if the turn rate is still changing, it indicates that there are other reasons for the change of turn rate. Then, the turn rate assistance subsystem starts and helps the driver control the turn rate at the desired value.

**Course assistance subsystem:** Relative sensors are working to monitor the action of driver on handle of rudders when rudder angle is zero. If the driver releases the handle, it means the driver wishes to remain at the current course angle subjectively. In this case, if the course angle is still changing, it indicates that there are other reasons for the change of course angle. Then, the course assistance subsystem starts and helps the driver control the course angle at the desired value.

#### 3.3. DAS controller

##### 3.3.1. Speed and turn rate controller

We define the following speed and turn rate control errors:

$$e_u = u - u_d \quad (9)$$

$$e_r = r - r_d \quad (10)$$

where  $u_d$ ,  $r_d$  are desired values.

Using (2), (9) and (10), the time derivatives of  $e_u$  and  $e_r$  are expressed as

$$\dot{e}_u = vr + \frac{1}{m}(\rho_a V_a Q \cos \beta + \vartheta_u(V_a, \beta) + 2F_{x_R} + \tau_{F_x}) - \dot{u}_d \quad (11)$$

$$\dot{e}_r = \frac{1}{J_z} \left( \rho_a V_a Q x_m \sin \beta + \rho_a V_a Q y_m \cos \beta + \vartheta_r(V_a, \beta, \Phi) + \tau_{M_z} \right) - \dot{r}_d \quad (12)$$

where

$$\begin{aligned} \vartheta_u(V_a, \beta) &= -0.5\rho_a V_a^2 C_{x_a} S_{PP} + (0.5\rho_w V_a^2 C_{sk} (h/l_{sk})^{-0.34} l_{sk} S_c^{0.5} \\ &\quad + 2.8167 C_{wm} p_c^{1.741} B_c / \rho_w g l_c^{-0.259}) \cos \beta \end{aligned} \quad (13)$$

$$\begin{aligned} \vartheta_r(V_a, \beta, \Phi) &= -0.5\rho_a V_a^2 C_{mz_a} S_{HP} H_{hov} - 0.5\rho_a V_a^2 C_{y_a} S_{LP} x_a \\ &\quad - 0.5\rho_a V_a^2 C_{x_a} S_{PP} y_a \\ &\quad + C_{wm} p_c^2 (B_c x_{wm} \sin \beta / \rho_w g + B_c y_{wm} \cos \beta / \rho_w g) \\ &\quad + (0.5\rho_w V_a^2 C_{sk} (h/l_{sk})^{-0.34} l_{sk} S_c^{0.5} + 2.8167 C_{wm} p_c^{1.741} B_c / (\rho_w g l_c)^{-0.259}) \\ &\quad - C_{wm} p_c^2 B_c / \rho_w g (x_{sk} \sin \beta + y_{sk} \cos \beta) \\ &\quad + 2l_c \varphi p_c x_c (0.5B_c \tan \Phi + h_0) \end{aligned} \quad (14)$$

Values  $C_{x_a}$ ,  $C_{y_a}$ ,  $C_{mz_a}$ ,  $C_{sk}$ ,  $C_{wm}$ ,  $\phi$ ,  $p_c$  in  $\vartheta_u(V_a, \beta)$ ,  $\vartheta_r(V_a, \beta, \Phi)$  mean the real parameters of the ACV.

In order to effectively deal with these parameters' uncertainties caused by the limitation of test, the error of manual record, the measurement error of instrument and etc., model knowledge neural network (MKNN) is proposed in this paper.

Learnable parameters  $\xi_i$ ,  $i = 1, 2, 3, 4, 5, 6, 7, 8, 9$  of MKNN are defined as follows:

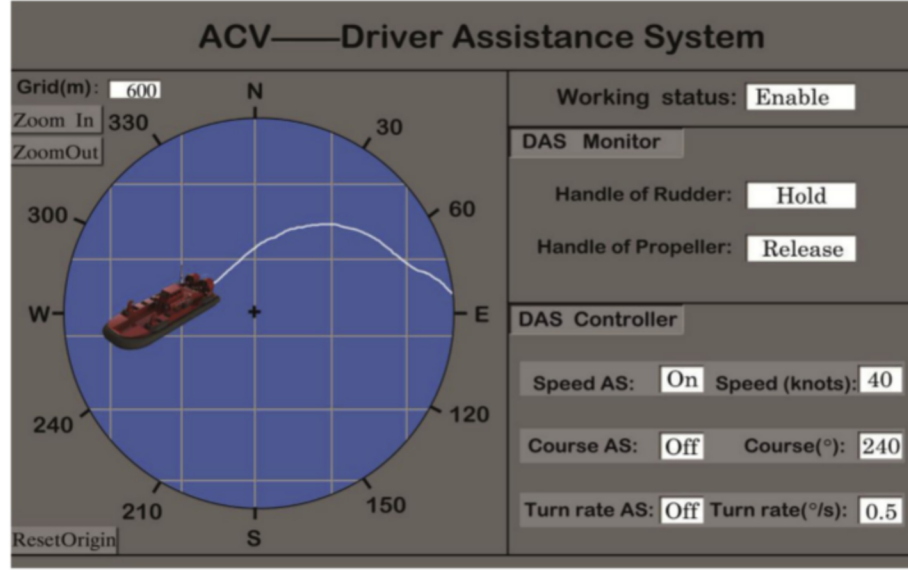


Fig. 3. The human-computer interface.

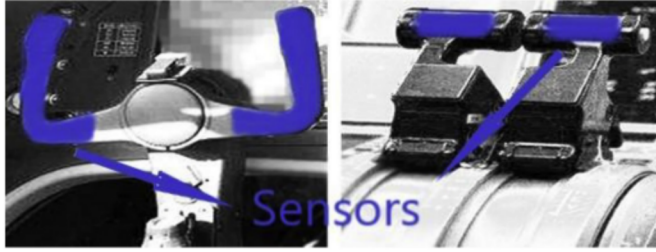


Fig. 4. Sensors position on handles of rudders and propellers.

$$\begin{cases} \xi_1 \text{ learning } \xi_1^* = C_{xa} \\ \xi_2 \text{ learning } \xi_2^* = C_{sk} \\ \xi_3 \text{ learning } \xi_3^* = C_{wm}p_c^{1.741} \\ \xi_4 \text{ learning } \xi_4^*: d(t) \end{cases} \quad \begin{cases} \xi_5 \text{ learning } \xi_5^* = C_{mza} \\ \xi_6 \text{ learning } \xi_6^* = C_{ya} \\ \xi_7 \text{ learning } \xi_7^* = C_{wm}p_c^{1.741} \\ \xi_8 \text{ learning } \xi_8^* = \phi p_c \\ \xi_9 \text{ learning } \xi_9^*: d(t) \end{cases} \quad (15)$$

where  $\xi_i^*$ ,  $i = 1, 2, 3, 4, 5, 6, 7, 8, 9$  are ideal learnable parameters,  $d(t)$  is unknown disturbance.

And the structure of MKNN is shown in Fig. 5. The uncertainty self-learning laws of parameters  $\xi$  will be given later.

From (13)–(15), (11) and (12) can be rewritten as

$$\begin{aligned} \dot{e}_u &= vr + \frac{1}{m}(-0.5\rho_a V_a^2 \xi_1^* S_{PP} + \rho_a V_a Q \cos \beta \\ &\quad + (0.5\rho_w V_a^2 \xi_2^* (h/l_{sk})^{-0.34} l_{sk} S_c^{0.5} \\ &\quad + 2.8167 \xi_3^* B_c / \rho_w g l_c^{-0.259}) \cos \beta + \xi_4^* + 2F_{xR} + \tau_{Fx}) - \dot{u}_d \end{aligned} \quad (16)$$

$$\begin{aligned} \dot{e}_r &= \frac{1}{J_z} (-0.5\rho_a V_a^2 \xi_5^* S_{HP} H_{hov} - 0.5\rho_a V_a^2 \xi_6^* S_{LP} x_a - 0.5\rho_a V_a^2 \xi_1^* S_{PP} y_a \\ &\quad + \rho_a V_a Q x_m \sin \beta + \rho_a V_a Q y_m \cos \beta + \xi_7^* (B_c x_{wm} \sin \beta / \rho_w g + B_c y_{wm} \cos \beta / \rho_w g) \\ &\quad + (0.5\rho_w V_a^2 \xi_2^* (h/l_{sk})^{-0.34} l_{sk} S_c^{0.5} + 2.8167 \xi_3^* B_c / (\rho_w g l_c^{-0.259})) \\ &\quad - \xi_7^* B_c / \rho_w g) (x_{sk} \sin \beta + y_{sk} \cos \beta) \\ &\quad + 2l_c \xi_8^* x_c (0.5B_c \tan \Phi + h_0) + \xi_9^* + \tau_{Mc}) - \dot{r}_d \end{aligned} \quad (17)$$

The following Lyapunov function is defined:

$$V = \frac{1}{2} e_u^2 + \frac{1}{2} e_r^2 + \frac{1}{2\gamma} \left( \sum_{i=1}^9 \xi_i^2 \right) \quad (18)$$

where  $\xi_i = \xi_i^* - \xi_i$ ,  $i = 1, 2, 3, 4, 5, 6, 7, 8, 9$ .

Then  $\dot{V}$  can be expressed as

$$\begin{aligned} \dot{V} &= e_u \dot{e}_u + e_r \dot{e}_r - \frac{1}{\gamma} \left( \sum_{i=1}^9 \xi_i \dot{\xi}_i \right) \\ &= e_u vr + e_u \left( \frac{1}{m} (-0.5\rho_a V_a^2 \xi_1^* S_{PP} + \rho_a V_a Q \cos \beta \right. \\ &\quad \left. + (0.5\rho_w V_a^2 \xi_2^* (h/l_{sk})^{-0.34} l_{sk} S_c^{0.5} + 2.8167 \xi_3^* B_c / (\rho_w g l_c^{-0.259})) \cos \beta + \xi_4^* + 2F_{xR} \right. \\ &\quad \left. + \tau_{Fx} - \dot{u}_d \right) + e_r \left( \frac{1}{J_z} (-0.5\rho_a V_a^2 \xi_5^* S_{HP} H_{hov} - 0.5\rho_a V_a^2 \xi_6^* S_{LP} x_a - 0.5\rho_a V_a^2 \xi_1^* S_{PP} y_a \right. \\ &\quad \left. + \rho_a V_a Q x_m \sin \beta + \rho_a V_a Q y_m \cos \beta + \xi_7^* (B_c x_{wm} \sin \beta / \rho_w g + B_c y_{wm} \cos \beta / \rho_w g) \right. \\ &\quad \left. + (0.5\rho_w V_a^2 \xi_2^* (h/l_{sk})^{-0.34} l_{sk} S_c^{0.5} + 2.8167 \xi_3^* B_c / (\rho_w g l_c^{-0.259})) \right. \\ &\quad \left. - \xi_7^* B_c / \rho_w g) (x_{sk} \sin \beta + y_{sk} \cos \beta) + 2l_c \xi_8^* x_c (0.5B_c \tan \Phi + h_0) + \xi_9^* + \tau_{Mc} \right) - \dot{r}_d - \frac{1}{\gamma} \left( \sum_{i=1}^9 \xi_i \dot{\xi}_i \right) \end{aligned} \quad (19)$$

The control laws are designed as

$$\begin{aligned} \tau_{Fx} &= m\dot{u}_d - mvr - mk_u e_u + 0.5\rho_a V_a^2 \xi_1^* S_{PP} - \rho_a V_a Q \cos \beta - 2F_{xR} \\ &\quad - 0.5\rho_w V_a^2 \xi_2^* (h/l_{sk})^{-0.34} l_{sk} S_c^{0.5} \cos \beta - 2.8167 \xi_3^* B_c \cos \beta / \rho_w g l_c^{-0.259} - \xi_4 \end{aligned} \quad (20)$$

$$\begin{aligned} \tau_{Mc} &= J_z \dot{r}_d - J_z k_r e_r + 0.5\rho_a V_a^2 \xi_5^* S_{HP} H_{hov} + 0.5\rho_a V_a^2 \xi_6^* S_{LP} x_a + 0.5\rho_a V_a^2 \xi_1^* S_{PP} y_a \\ &\quad - \rho_a V_a Q x_m \sin \beta - \rho_a V_a Q y_m \cos \beta + \xi_7^* (B_c x_{wm} \sin \beta / \rho_w g + B_c y_{wm} \cos \beta / \rho_w g) \\ &\quad + (0.5\rho_w V_a^2 \xi_2^* (h/l_{sk})^{-0.34} l_{sk} S_c^{0.5} + 2.8167 \xi_3^* B_c / (\rho_w g l_c^{-0.259})) \\ &\quad - \xi_7^* B_c / \rho_w g) (x_{sk} \sin \beta + y_{sk} \cos \beta) - 2l_c \xi_8^* x_c (0.5B_c \tan \Phi + h_0) - \xi_9 \end{aligned} \quad (21)$$

where  $k_u, k_r > 0$ .

The uncertainty self-learning laws are designed as

$$\begin{aligned} \dot{\xi}_1 &= \frac{\gamma e_u}{m} (-0.5\rho_a V_a^2 S_{PP}), & \dot{\xi}_4 &= \frac{\gamma e_u}{m} \\ \dot{\xi}_2 &= \frac{\gamma e_u}{m} 0.5\rho_w V_a^2 (h/l_{sk})^{-0.34} l_{sk} S_c^{0.5} \cos \beta, & \dot{\xi}_5 &= \frac{\gamma e_r}{J_z} (-0.5\rho_a V_a^2 S_{HP} H_{hov}) \\ \dot{\xi}_3 &= \frac{\gamma e_u}{m} 2.8167 B_c \cos \beta / (\rho_w g l_c^{-0.259}), & \dot{\xi}_6 &= \frac{\gamma e_r}{J_z} (-0.5\rho_a V_a^2 S_{LP} x_a) \\ \dot{\xi}_7 &= \frac{\gamma e_r}{J_z} \rho_w g (x_{wm} \sin \beta + y_{wm} \cos \beta - x_{sk} \sin \beta - y_{sk} \cos \beta) \\ \dot{\xi}_8 &= \frac{\gamma e_r}{J_z} 2l_c x_c (0.5B_c \tan \Phi + h_0), & \dot{\xi}_9 &= \frac{\gamma e_r}{J_z} \end{aligned} \quad (22)$$

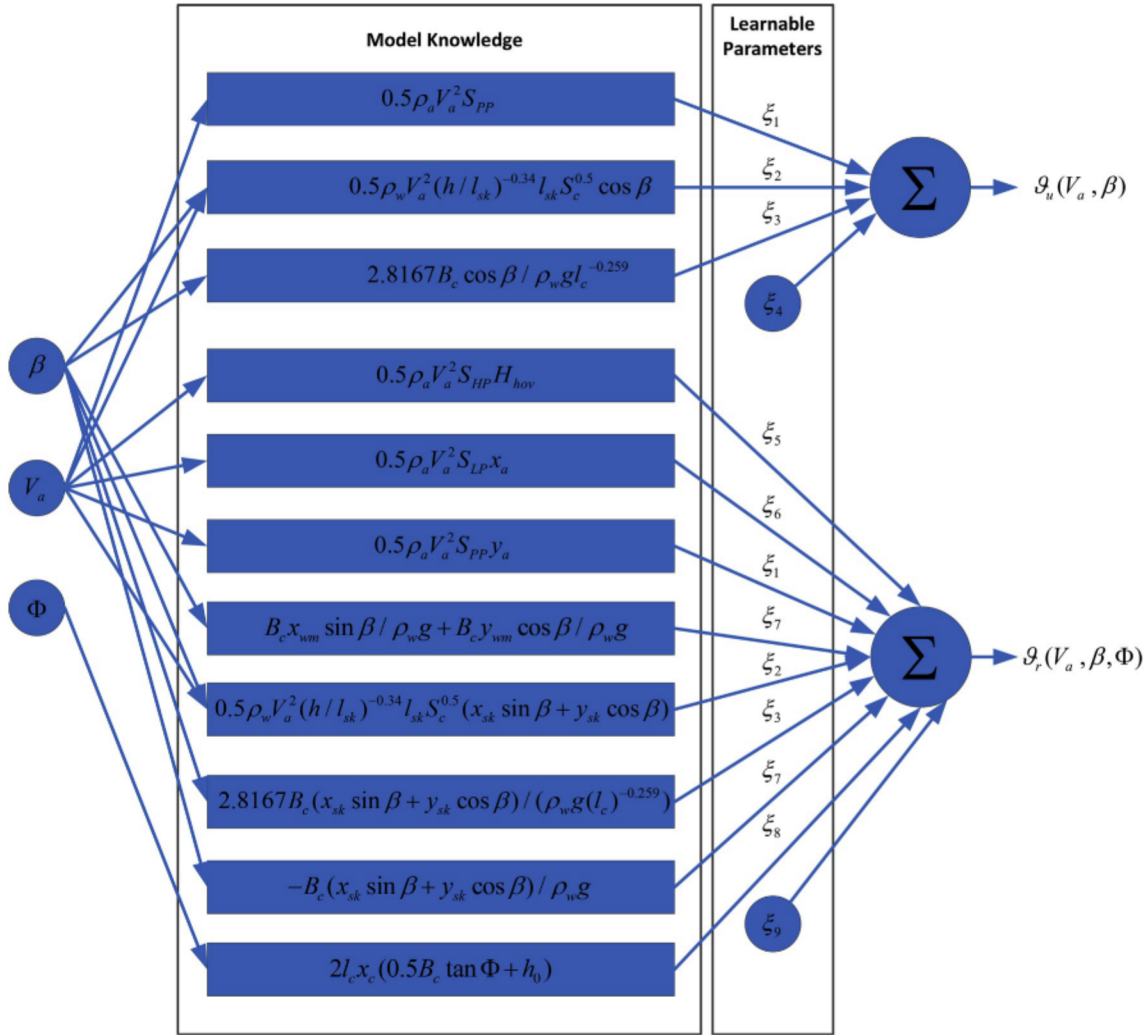


Fig. 5. Structure of MKNN

where  $\gamma > 0$ .

Substituting (20)–(22) into (19), we have

$$\dot{V} = -k_u e_u^2 - k_r e_r^2 < 0, \text{ if } e_u \neq 0 \text{ and } e_r \neq 0$$

Integrating both sides of (23), we obtain

$$\begin{aligned} V(t) - V(0) &= \int_0^t (-k_u e_u^2 - k_r e_r^2) dt \\ 0 \leq V(t) &= V(0) - \int_0^t (k_u e_u^2 + k_r e_r^2) d\tau \leq V(0) < \infty \\ V(0) &= V(t) + \int_0^t (k_u e_u^2 + k_r e_r^2) d\tau \\ &\geq \int_0^t (k_u e_u^2 + k_r e_r^2) d\tau \end{aligned} \quad (24)$$

So

$$\lim_{t \rightarrow \infty} \int_0^t (k_u e_u^2 + k_r e_r^2) d\tau \leq V(0) < \infty \quad (25)$$

According to Barbalat's lemma, we have  $\lim_{t \rightarrow \infty} e_u = 0$  and  $\lim_{t \rightarrow \infty} e_r = 0$ .

### 3.3.2. Course controller

From Fig. 2, we have

$$\sigma = \psi + \beta \quad (26)$$

Then the course error and its derivative are given as

$$e_\sigma = \sigma - \sigma_d = \psi + \beta - \sigma_d \quad (27)$$

$$\dot{e}_\sigma = \dot{\sigma} - \dot{\sigma}_d = r + \dot{\beta} - \dot{\sigma}_d \quad (28)$$

Considering the following Lyapunov function candidate:

$$V_\sigma = \frac{1}{2} e_\sigma^2 \quad (29)$$

The time derivative of  $V_\sigma$  is as follows

$$\dot{V}_\sigma = e_\sigma \dot{e}_\sigma = e_\sigma (r + \dot{\beta} - \dot{\sigma}_d) \quad (30)$$

Let  $r$  be the virtual control input and if it satisfies  $r = -\dot{\beta} + \dot{\sigma}_d - k_\sigma e_\sigma$ , then we have

$$\dot{V}_\sigma = -k_\sigma e_\sigma^2 < 0, \text{ if } e_\sigma \neq 0 \quad (31)$$

Hence, if the desired turn rate in (10) is chosen as  $r_d = -\dot{\beta} + \dot{\sigma}_d - k_\sigma e_\sigma$ , and the turn rate error  $e_r$  converges to zero under the control of turn rate assistance subsystem, we have  $r = -\dot{\beta} + \dot{\sigma}_d - k_\sigma e_\sigma$ . Then the convergence of  $e_\sigma$  to zero is guaranteed from (31).

## 4. Simulations

### 4.1. Purposes

Simulations are divided into two cases. And in each case, there are three different situations such as situation 1, situation 2 and situation 3. Simulation purposes are as follows:

- Verify the effectiveness of the speed and course assistance

**Table 1**  
Main particulars of ACV.

m(kg)	40000	$J_z(\text{kgm}^2)$	$1.8 \times 10^6$	$J_x(\text{kgm}^2)$	$2.5 \times 10^5$
$S_{PP}(\text{m}^2)$	45	$S_{LP}(\text{m}^2)$	93	$S_{HP}(\text{m}^2)$	230
$S_c(\text{m}^2)$	205	$l_{sk}(\text{m})$	65	$l_c(\text{m})$	23.6
$B_c(\text{m})$	8.9	$H_{hov}(\text{m})$	5.9	$h_0(\text{m})$	1.3
$h(\text{m})$	1	$h_m(\text{m})$	2.4	$g(\text{m/s}^2)$	9.8
$V_w(\text{knots})$	5	$\beta_w(\text{deg})$	45		

**Table 2**  
Input parameters and coefficients of ACV.

$C_{x_a}$	1.05	$C_{y_a}$	1	$(x_m, y_m, z_m)$	(3.0, -0.8)
$C_{mx_a}$	0.9	$C_{mza}$	1.02	$(x_{wm}, y_{wm}, z_{wm})$	(2.8, 0.1, 5)
$C_{wm}$	$N_{wm}(u)$	$C_{sk}$	1.2	$(x_a, y_a, z_a)$	(2.8, 0.0, 3)
$C_{xR}/C_{yR}$	0.52	$\phi$	0.3	$(x_{sk}, y_{sk}, z_{sk})$	(2.8, 0, 1)
$Q(\text{m}^3/\text{s})$	145	$p_c(\text{N/m}^2)$	2000	$(x_c, y_c, z_c)$	(2.8, 0, 1.5)
$\rho_a(\text{kg/m}^3)$	1.29	$\rho_w(\text{kg/m}^3)$	1025	$(x_R, y_{R1}, y_{R2}, z_R)$	(-9.3, -3, -1.5)

\*More information about the coefficients in Table 2 can be found in (Yun and Bliault, 2000).

subsystems of the DAS by comparing situation 1 with situation 2 and 3 in case 1.

- Verify the effectiveness of the speed and turn rate assistance subsystems of the DAS by comparing situation 1 with situation 2 and 3 in case 2.
- Verify the superiority of the DAS with MKNN-based controller in situation 3 by comparing the control performance of DAS with ordinary controller in situation 2 in both two cases.

#### 4.2. Scheme

The first case is about the verification of the speed and course assistance subsystems. The other is about the speed and turn rate assistance subsystems. In each case, a comparison of three different situations is conducted.

Situation 1. No DAS, that is DAS is not used. The ACV is operated only by driver's manual operation. Force and moment of actuators are operated as follows

$$\begin{aligned} \text{case 1: } & \tau_{F_x} = 4.08 \times 10^5 \text{ N}, \tau_{M_z} = 0 \\ \text{case 2: } & \tau_{F_x} = 4.08 \times 10^5 \text{ N}, \tau_{M_z} = -2.45 \times 10^5 \text{ Nm} \end{aligned} \quad (32)$$

Situation 2. DAS with ordinary controller, that is an ordinary controller as shown in (33) and (34) is used as DAS controller. Parameter uncertainty is not considered in this controller.

$$\begin{aligned} \tau_{F_x} = & m\dot{u}_d - m\lambda_1 e_u - mvr - mk_u s_u - 0.5\rho_a V_a^2 \bar{C}_{x_a} S_{PP} - \rho_a V_a Q \cos \beta \\ & - 0.5\rho_w V_a^2 \bar{C}_{sk} (h/l_{sk})^{-0.34} l_{sk} S_c^{0.5} \cos \beta - 2.8167 \bar{C}_{wm} \bar{p}_c^{1.741} B_c \cos \beta \\ & / \rho_w g l_c^{-0.259} \end{aligned} \quad (33)$$

$$\begin{aligned} \tau_{M_z} = & J_z \dot{r}_d - J_z \lambda_2 e_r - J_z k_r s_r - 0.5\rho_a V_a^2 \bar{C}_{mza} S_{HP} H_{hov} - 0.5\rho_a V_a^2 \bar{C}_{y_a} S_{LP} x_a \\ & - 0.5\rho_a V_a^2 \bar{C}_{x_a} S_{PP} y_a \\ & - \rho_a V_a Q x_m \sin \beta - \rho_a V_a Q y_m \cos \beta + \bar{C}_{wm} \bar{p}_c^{2} (B_c x_{wm} \sin \beta / \rho_w g \\ & + B_c y_{wm} \cos \beta / \rho_w g) \\ & + (0.5\rho_w V_a^2 \bar{C}_{sk} (h/l_{sk})^{-0.34} l_{sk} S_c^{0.5} + 2.8167 \bar{C}_{wm} \bar{p}_c^{1.741} B_c / (\rho_w g l_c^{-0.259})) \\ & - \bar{C}_{wm} \bar{p}_c^{2} B_c / \rho_w g)(x_{sk} \sin \beta + y_{sk} \cos \beta) - 2l_c \phi \bar{p}_c x_c (0.5B_c \tan \phi + h_0) \end{aligned} \quad (34)$$

where  $\bar{C}_{x_a}$ ,  $\bar{C}_{y_a}$ ,  $\bar{C}_{mza}$ ,  $\bar{C}_{sk}$ ,  $\bar{C}_{wm}$ ,  $\bar{p}_c$  are measured values through tank test, wind tunnel test and sensors. To express their uncertainties and measurement errors, they are given as follows

$$\begin{cases} \bar{C}_{x_a} = C_{x_a} + 0.2|C_{x_a}| \sin(0.01t) \\ \bar{C}_{y_a} = C_{y_a} + 0.15|C_{y_a}| \cos(0.03t) \\ \bar{C}_{mza} = C_{mza} + 0.3|C_{mza}| \cos(0.02t) \\ \bar{C}_{sk} = C_{sk} + 0.09|C_{sk}| \sin(0.05t) \\ \bar{C}_{wm} = C_{wm} + 0.1|C_{wm}| \cos(0.15t) \\ \bar{p}_c = p_c + 0.12|p_c| \sin(0.04t) \end{cases} \quad (35)$$

Situation 3. DAS with MKNN-based controller, that is the proposed MKNN-based controller (20)–(22) is adopted as DAS controller.

For both situation 2 and 3, when  $t < 200\text{s}$ ,  $\tau_{F_x}$  and  $\tau_{M_z}$  are given by (32). Then driver releases handles and the DAS starts working from  $t = 200\text{s}$ .  $\tau_{F_x}$  and  $\tau_{M_z}$  are generated by the corresponding DAS controller.

In all situations, the time-varying disturbances (Wang et al., 2018; Du et al., 2016) as shown in (36) are taken as unknown disturbance.

$$d(t) = J(\psi, \Phi)^T b \quad (36)$$

where

$$J(\psi, \Phi) = \begin{bmatrix} \cos \psi & -\sin \psi \cos \Phi & 0 & 0 \\ \sin \psi & \cos \psi \cos \Phi & 0 & 0 \\ 0 & 0 & 1 & 0 \\ 0 & 0 & 0 & \cos \Phi \end{bmatrix}$$

$\dot{b} = -T^{-1}b + Aw$  is the first-order Markov process,  $b \in R^4$  is the vector of bias forces and moment,  $T \in R^{4 \times 4}$  is the diagonal time constant matrix,  $w \in R^4$  is the vector of zero-mean Gaussian white noises, and  $A \in R^{4 \times 4}$  is a diagonal matrix scaling the amplitude of  $w$ .

**Table 3**  
Use of DAS and its controller in simulations.

Situation	DAS	DAS controller	Results
1	Do not use	–	Figures of case 1: 6A,7,
2	Use	Case 1: Ordinary controllers (33) and (34) with $r_d = -\dot{\beta} + \dot{\phi}_d - k_\sigma(\psi + \beta - \sigma_d)$ Case 2: Ordinary controllers (33) and (34)	8A-14A Figures of case 2: 6B,8B-14B
3	Use	Case 1: MKNN-based controllers (20) and (21) with $r_d = -\dot{\beta} + \dot{\phi}_d - k_\sigma(\psi + \beta - \sigma_d)$ , and uncertainty self-learning laws (22) Case 2: MKNN-based controllers (20) and (21), and uncertainty self-learning laws (22)	

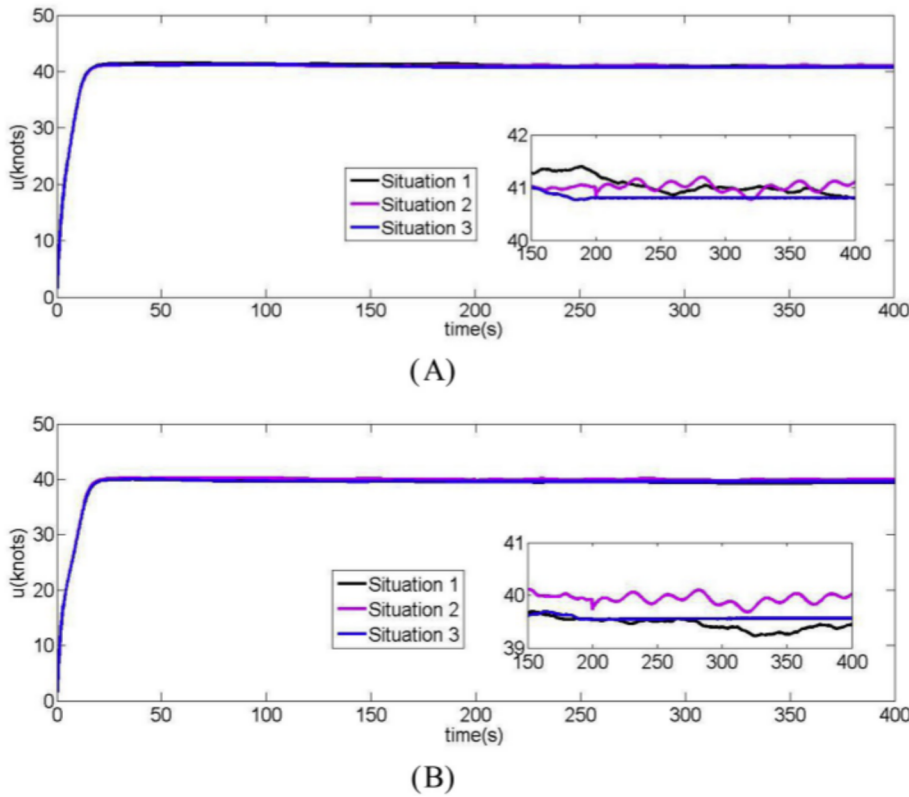


Fig. 6. Speed of ACV in two cases: (6A) corresponds to case 1. (6B) corresponds to case 2.

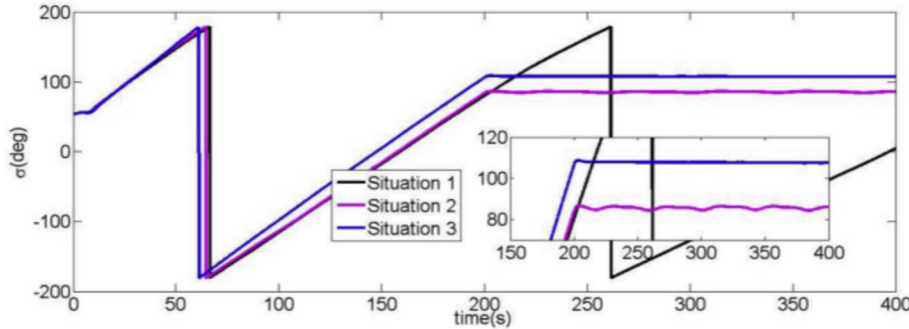


Fig. 7. Course angle of ACV in case 1.

#### 4.3. Parameters

The main particulars of ACV are shown in Table 1. The other input parameters and coefficients are shown in Table 2.

And the following function  $N_{wm}(u)$  is selected to represent the relationship between  $C_{wm}$  and  $u$  according to the corresponding relationship curve in third chapter of (Yun and Bliault, 2000).

$$N_{wm}(u) = 0.3e^{\left(\frac{(u-10)^2}{2 \times 8^2}\right)} + 0.2$$

Choose  $b(0) = [1 \times 10^4 N, 1 \times 10^4 N, 1 \times 10^4 Nm, 1 \times 10^4 Nm]^T$ ,  $T = diag(10^3, 10^3, 10^3, 10^3)$ , and  $A = diag(5000, 5000, 5000, 5000)$ .

The initial values of ACV are.

$$\begin{aligned} x(0) &= -500, y(0) = 200, \Phi(0) = 0, \psi(0) = 50^\circ, \\ u(0) &= 0, v(0) = 0, p(0) = 0, r(0) = 0. \end{aligned}$$

#### 4.4. Results

In case 1, the desired speed and course angle are the values

at  $t = 200$  s for situations 2 and 3. And in case 2, the desired speed and turn rate are the values at  $t = 200$  s for situations 2 and 3. Controllers used in different situations are shown in Table 3.

Among them, Figs. 6–10 show the motion states of ACV in case 1 and 2. The input force and moment are shown by Figs. 11 and 12. The generated disturbance of situation 3 in case 1 and case 2 are shown by Fig. 13. It is worth noting that the disturbance of situation 1 and 2 are slight different from situation 3 due to the randomness of zero-mean Gaussian white noises. For the sake of brevity, they are not shown here. And self-learning parameters are shown in Fig. 14.

It is obvious from Figs. 6–8 that although the force and moment of actuators of situation 1 in both two cases are remain unchanged, but the speed, course angle and turn rate of situation 1 are not stable because of the disturbance.

And for situation 2 in both cases, the DAS with ordinary controller starts working at  $t = 200$  s. Then the stability of the speed is improved from  $t = 200$  s as shown in Fig. 6 by the speed controller of DAS. Similarly, the stability of turn rate is improved by the turn rate controller in Fig. 8. And the course keeping is realized from Fig. 7. However, it is

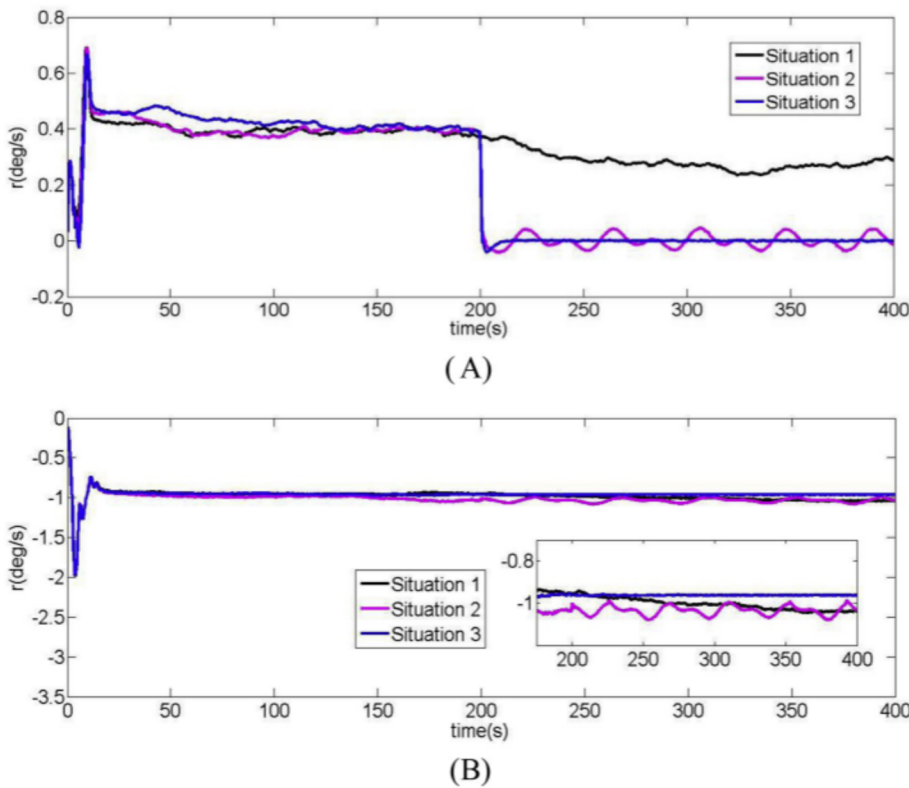


Fig. 8. Turn rate of ACV in two cases: (8A) corresponds to case 1. (8B) corresponds to case 2.

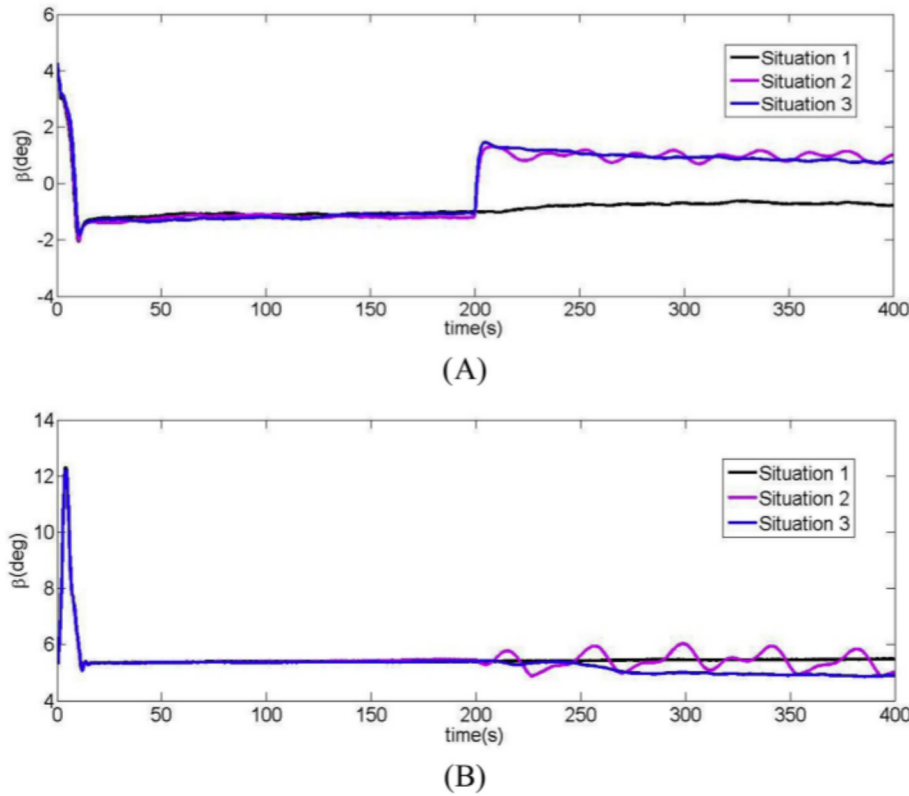


Fig. 9. Drift angle of ACV in two cases: (9A) corresponds to case 1. (9B) corresponds to case 2.

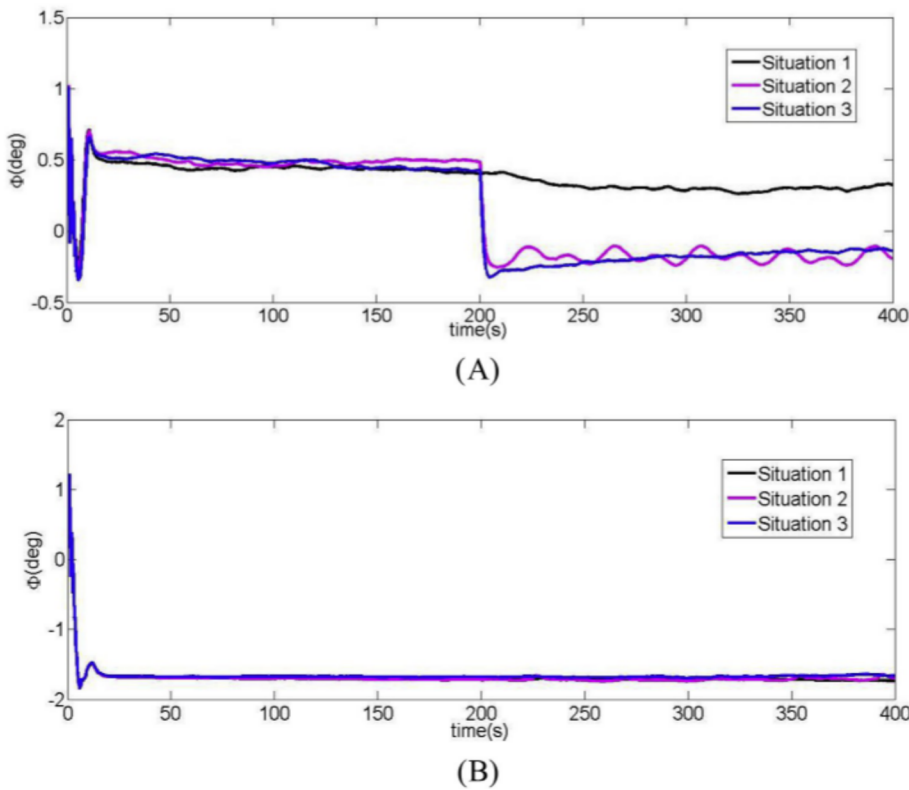


Fig. 10. Roll angle of ACV in two cases: (10A) corresponds to case 1. (10B) corresponds to case 2.

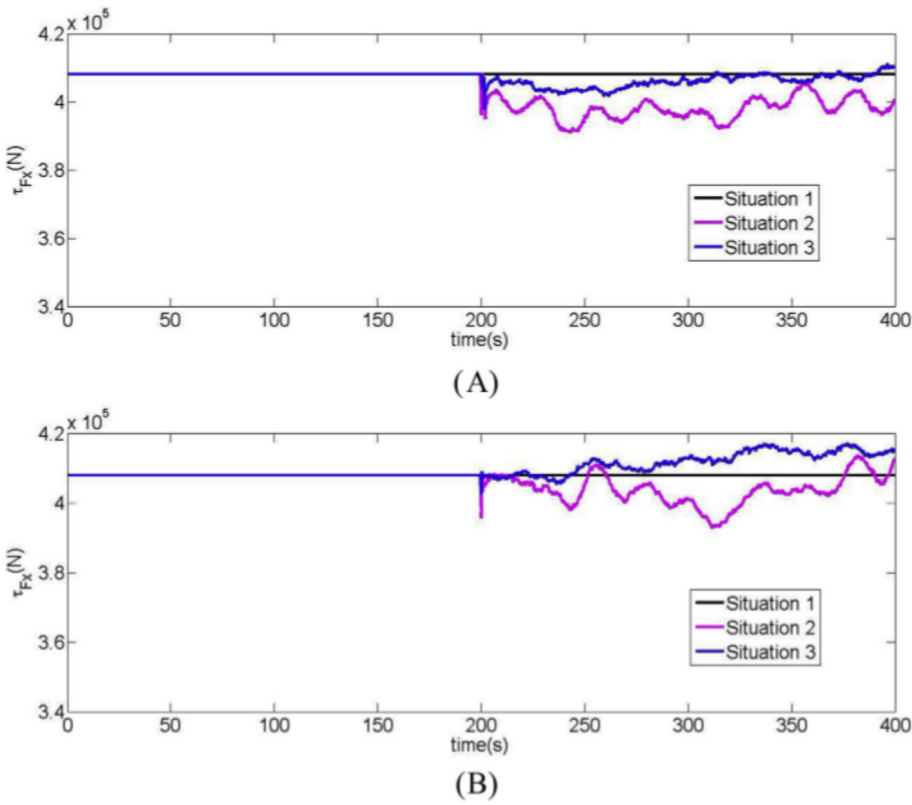


Fig. 11. Surge control law in two cases: (11A) corresponds to case 1. (11B) corresponds to case 2.

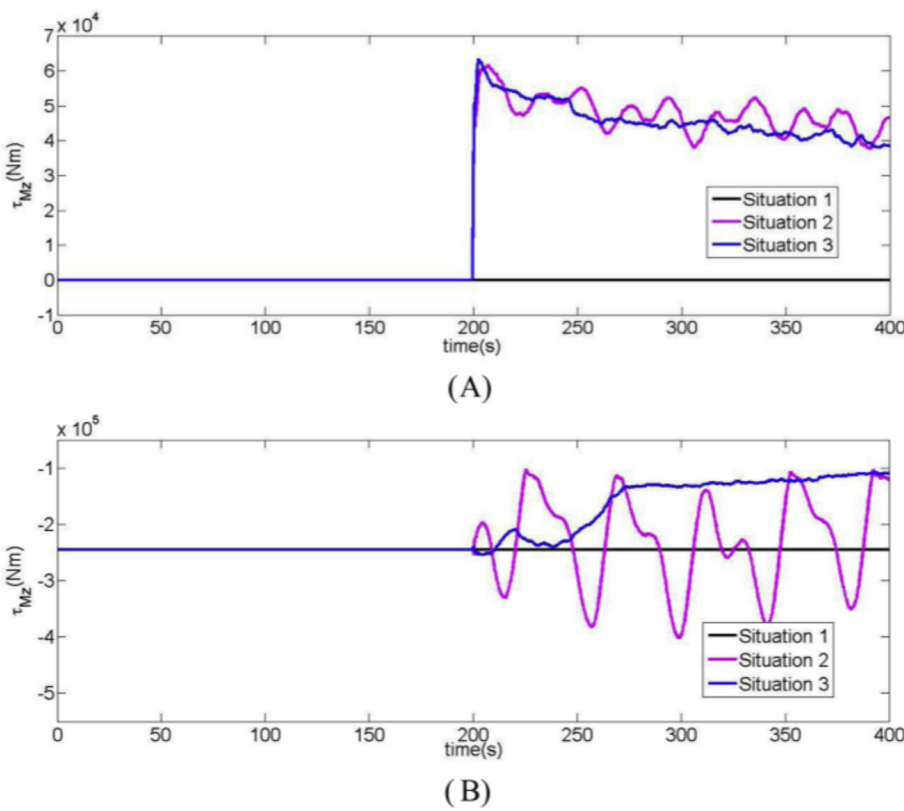


Fig. 12. Yaw control law in two cases: (12A) corresponds to case 1. (12B) corresponds to case 2.

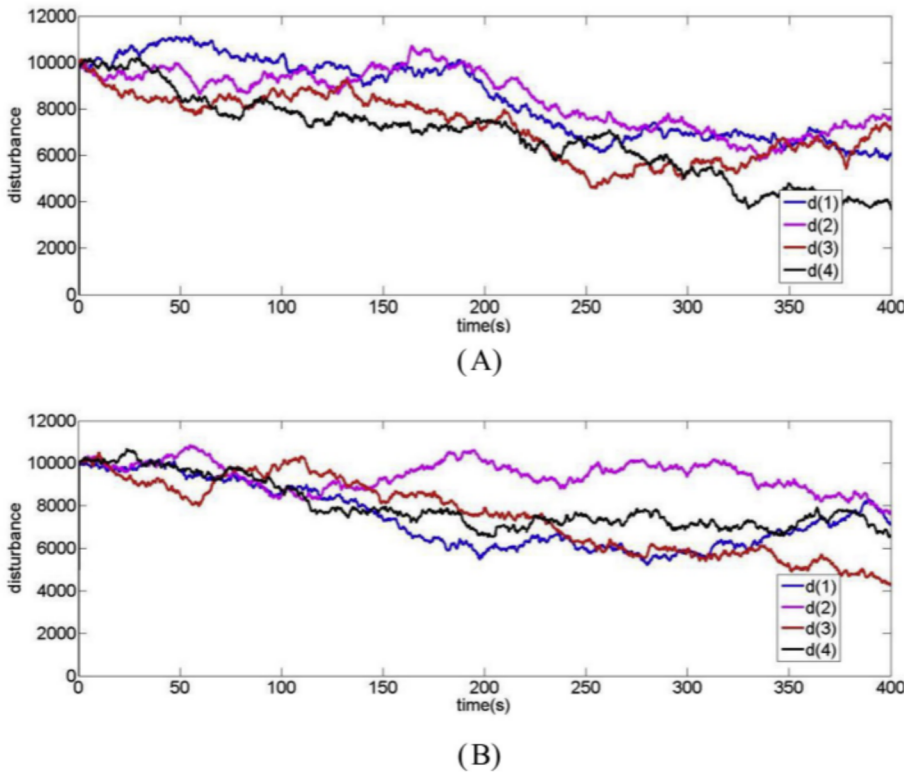


Fig. 13. Disturbance of Situation 3 in two cases: (13A) corresponds to case 1. (13B) corresponds to case 2.

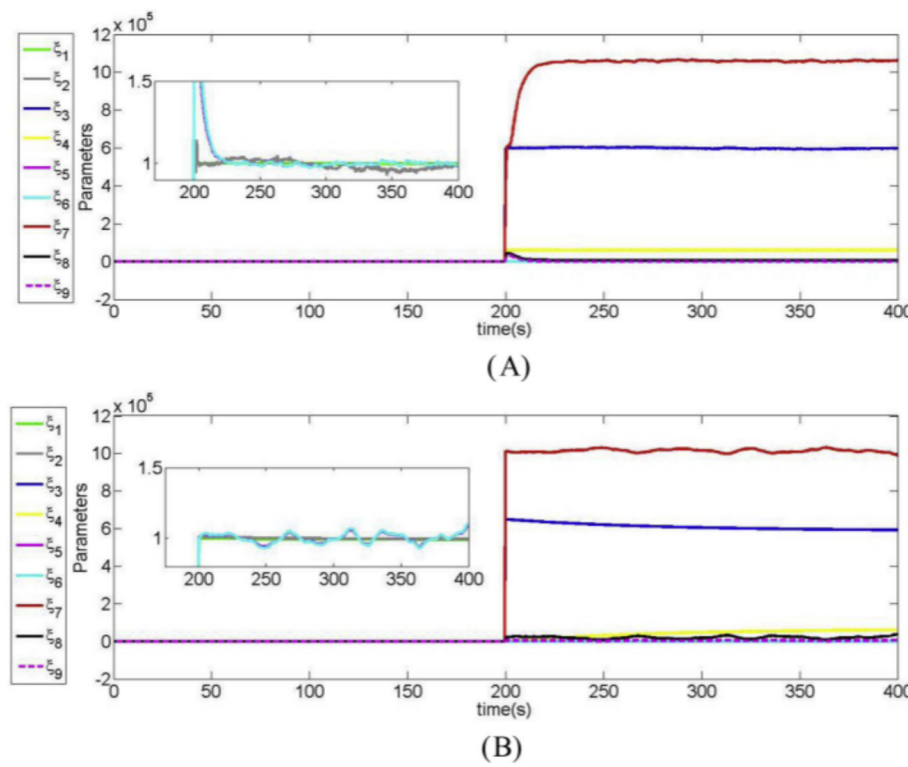


Fig. 14. Self-learning parameters in two cases: (14A) corresponds to case 1, (14B) corresponds to case 2.

obvious that the control performance of situation 2 is unsatisfied and large errors are existed. The reason is the DAS controller used in situation 2 of both two cases is designed based on a parameter uncertainty model.

In situation 3 of two cases, the DAS with MKNN-based controller are adopted. It is undeniable from the comparisons of Figs. 6–8 that the DAS with MKNN-based controller is better than DAS with ordinary controller in situation 2. It can help drivers control the states stay on the values from  $t = 200$ s with small enough errors although the unknown disturbance and parameter uncertainty are existed.

## 5. Conclusion

In this paper, a DAS including an intuitive human-computer interface, DAS monitor and DAS controller is developed for ACV. The human-computer interface is easy to be understood and used for humans. And DAS monitor can monitor driver's operational changes. For the DAS controller part, MKNN method is first proposed in this paper to deal with parameter uncertainty. Then the MKNN-based controller is designed as the DAS controller. The developed DAS can assist drivers in better control operations according to their action instructions. The simulations indicate the effectiveness of the DAS. Moreover, the superiority of DAS with MKNN-based controller is verified by comparing with DAS with ordinary controller.

## Conflicts of interest

The authors declare that there are no conflicts of interest regarding the publication of this paper.

## Acknowledgments

The supports of the National Natural Science Foundation of China (Grant no. 51309062) and the project “Research on Maneuverability of High Speed Hovercraft” (Project no. 2007DFR80320) are gratefully acknowledged.

## Appendix A. Supplementary data

Supplementary data to this article can be found online at <https://doi.org/10.1016/j.oceaneng.2018.12.001>.

## Nomenclatures

$\phi$	ACV's roll angle
$\psi$	ACV's yaw angle
$\beta$	ACV's drift angle
$\beta_a$	Relative wind direction
$\beta_w$	Absolute wind direction
$\phi$	Discharge coefficient
$\rho_a$	Air density
$\rho_w$	Water density
$B_c$	ACV's cushion beam
$C_{sk}$	Coefficient of skirt drag
$C_{wm}$	Coefficient of wave-making drag
$C_{x_a}, C_{y_a}, C_{mz_a}$	Coefficients of aerodynamic profile drag
$C_{x_R}C_{y_R}$	Coefficients of rudder force
$F_{xp}$	Surge force generated by an air propeller
$F_{x_R}, F_{y_R}$	Surge and sway force generated by an air rudder
$F_{x_a}, F_{y_a}$	Aerodynamic profile drag at surge and sway DOF
$F_m$	Air momentum drag
$F_{wm}$	Wave-making drag
$F_{sk}$	Skirt drag
$F_c$	Cushion force
$h$	Average clearance for air leakage in static hovering mode
$h_m$	Metacentric height
$h_0$	Initial lift height
$H_{hov}$	ACV's height
$J_x, J_z$	ACV's moment of inertia
$l_c$	ACV's cushion length
$l_{sk}$	Total peripheral length of the skirts
$m$	ACV's mass
$M_{x_R}, M_{z_R}$	Roll and yaw moment generated by an air rudder

$M_{x_a}, M_{z_a}$	Aerodynamic profile drag at roll and yaw DOF
$M_G$	Restoring moment during rolling
$p$	ACV's roll velocity
$p_c$	Cushion pressure
$Q$	Fan flow of cushion fans
$r$	ACV's yaw velocity
$S_{PF}$	Positive projection area
$S_{LP}$	Lateral projection area
$S_{HP}$	Horizontal projection area
$S_c$	ACV's cushion area
$u$	ACV's surge velocity
$v$	ACV's sway velocity
$V_a$	Relative wind speed
$V_w$	Absolute wind speed
$(x, y)$	Coordinates of ACV's center of mass
$(x_m, y_m, z_m)$	Coordinates of air momentum drag's acting point
$(x_{wm}, y_{wm}, z_{wm})$	Coordinates of wave-making drag's acting point
$(x_a, y_a, z_a)$	Coordinates of aerodynamic profile drag's acting point
$(x_k, y_k, z_k)$	Coordinates of skirt drag's acting point
$(x_c, y_c, z_c)$	Coordinates of cushion force's acting point
$(x_R, y_{R1}, y_{R2}, z_R)$	Coordinates of rudder force's acting point

## References

- Chen, JiaWang, Zhu, Huangchao, Zhang, Lei, Sun, Yuxia, 2018. Research on fuzzy control of path tracking for underwater vehicle based on genetic algorithm optimization. *Ocean Eng.* 156, 217–223.
- Cohen, M., Miloh, T., Zilman, G., 2001. Wave resistance of a hovercraft moving in water with nonrigid bottom. *Ocean Eng.* 28 (11), 1461–1478.
- Doctors, L.J., 1997. Optimal pressure distribution for river based air cushion vehicles. *Schiffstechnik* 44, 32–36.
- Doctors, L.J., Sharma, S.D., 1972. The wave resistance of an air cushion vehicle in steady and accelerated motion. *J. Ship Res.* 16, 248–260.
- Du, J., Hu, X., Sun, Y., 2016. Robust dynamic positioning of ships with disturbances under input saturation. *Automatica* 73 (C), 207–214.
- Dyachenko, V.K., 1999. Resistance Air Cushion Vehicle. Krylov Central Research Institute, Saint Petersburg, Russia.
- Feng, Jun, Wen, Guo-Xing, 2015. Adaptive NN consensus tracking control of a class of nonlinear multi-agent systems. *Neurocomputing* 151, 288–295.
- Fu, Mingyu, Gao, Shuang, Wang, Chenglong, 2017. Safety-guaranteed trajectory tracking control for the underactuated hovercraft with state and input constraints. *Math. Probl. Eng.*, 9452920 12 pages, 2017.
- Fu, Mingyu, Gao, Shuang, Wang, Chenglong, Li, Mingyang, July 10, 2018. Human-centered automatic tracking system for underactuated hovercraft based on adaptive chattering-free full-order terminal sliding mode control. In: IEEE ACCESS, <https://doi.org/10.1109/ACCESS.2018.2854752>.
- Hua, F., 2008. Analysis and Consideration on Safety of All-lift Hovercraft. SHIP & BOAT, Shanghai, China.
- Hwang, C.I., Chiang, C.C., Yeh, Y.W., 2014. Adaptive fuzzy hierarchical sliding-mode control for the trajectory tracking of uncertain underactuated nonlinear dynamic systems. *IEEE Trans. Fuzzy Syst.* 22 (2), 286–299.
- Jun, L., Huang, G., 2007. The four degree-of-freedom maneuverability of an air cushion vehicle. *J. Shanghai Jiao Tong Univ. (Sci.)* 41 (2), 216–220.
- Lin, X., Nie, J., Jiao, Y., et al., 2018. Adaptive fuzzy output feedback stabilization control for the underactuated surface vessel. *Appl. Ocean Res.* 74, 40–48.
- Liu, C., Zou, Z., Yin, J., 2015. Trajectory tracking of underactuated surface vessels based on neural network and hierarchical sliding mode. *J. Mar. Sci. Technol.* 20 (2), 322–330.
- Lu, Xingguo, Zhao, Yue, Liu, Ming, 2018. Self-learning interval type-2 fuzzy neural network controllers for trajectory control of a Delta parallel robot. *Neurocomputing* 283, 107–119.
- Morales, R., Sira-Ramírez, H., Somolinos, J.A., 2015. Linear active disturbance rejection control of the hovercraft vessel model. *Ocean Eng.* 96 (12), 100–108.
- Mu, D.D., Wang, G.F., Fan, Y.S., 2017. Design of adaptive neural tracking controller for pod propulsion unmanned vessel subject to unknown dynamics. *J. Electr. Eng. Tech.* 12 (6), 2365–2377.
- Newman, J.N., Poole, F.A.P., 1962. The wave resistance of a moving pressure distribution in a canal. *Schiffstechnik* 9, 1–6.
- Ni, J., Liu, L., He, W., et al., 2018. Adaptive dynamic surface neural network control for nonstrict-feedback uncertain nonlinear systems with constraints. *Nonlinear Dynam.* 1–20.
- Okita, N., Sahin, I., Hyman, M.C., 2001. Disturbance during steady and unsteady motion of a two-dimensional pressure distribution. *J. Ship Res.* 45, 165–176.
- Rigatos, G.G., Raffo, G.V., 2015. Input-output linearizing control of the underactuated hovercraft using the derivative-free nonlinear Kalman filter. *Unmanned Syst.* 3 (2), 127–142.
- Sahin, I., Hyman, M.C., 2001. Simulation of three-dimensional finite-depth wave phenomenon for moving pressure distributions. *Ocean Eng.* 28, 1621–1630.
- Sanchez, Mauricio A., Castillo, Oscar, Castro, Juan R., 2015. Generalized type-2 fuzzy systems for controlling a mobile robot and a performance comparison with interval type-2 and type-1 fuzzy systems. *Expert Syst. Appl.* 42, 5904–5914.
- Shojaei, K., Oct. 2015. Neural adaptive robust control of underactuated marine surface vehicles with input saturation. *Appl. Ocean Res.* 53, 267–278.
- Sira-Ramirez, H., Nov. 2002. Dynamic second-order sliding mode control of the hovercraft vessel. *IEEE Trans. Contr. Syst. Technol.* 10 (6), 860–865.
- Tao, M., Chengjie, W., 2012. Hovercraft Performance and Skirt-cushion System Dynamics Design. National Defence Industry Press, China.
- Tuck, E.O., Lazauskas, L., 2001. Free-surface distribution with minimum wave resistance. *ANZIAM J.* 4, E75–E101.
- Tuck, E.O., Scullen, D.C., Lazauskas, L., 2002. Wave pattern and minimum wave resistance for high-speed vessels. In: Proceedings 24th Symposium on Naval Hydrodynamics, pp. 23–39 Fukuoka, Japan, July.
- Wang, Yuzhong, Jin, Qibing, Zhang, Ridong, 2017. Improved fuzzy PID controller design using predictive functional control structure. *ISA (Instrum. Soc. Am.) Trans.* 71, 354–363.
- Wang, Y., Tuo, Y., Yang, S.X., et al., July 2018. Reliability-based robust dynamic positioning for a turret-moored floating production storage and offloading vessel with unknown time-varying disturbances and input saturation. *ISA Trans.* 78, 66–79.
- Xia, Kewei, Huo, Wei, 2016. Robust adaptive backstepping neural networks control for spacecraft rendezvous and docking with input saturation. *ISA (Instrum. Soc. Am.) Trans.* 62, 249–257.
- Xia, Jianwei, Zhang, Jing, Sun, Wei, Zhang, Baoyong, Wang, Zhen, 27 July 2018. Finite-time adaptive fuzzy control for nonlinear systems with full state constraints. In: IEEE Transactions on Systems, Man, and Cybernetics: Systems, <https://doi.org/10.1109/TSMC.2018.2854770>.
- Yun, L., Bliault, A., 2000. Theory and Design of Air Cushion Craft. Butterworth-Heinemann, Oxford, U.K.
- Zhang, G., Zhang, X., Zheng, Y., Aug. 2015. Adaptive neural path-following control for underactuated ships in fields of marine practice. *Ocean Eng.* 104, 558–567.
- Zhao, J., Pang, J., Jul. 2010. Trajectory control of underactuated hovercraft. *Proc. IEEE 8<sup>th</sup> World Congr. Intell. Control Automat.* 20 (1), 3904–3907.
- Zilman, G., 1993. Mathematical simulation of hovercraft maneuvering. In: Proceedings of the Twenty- Third American Towing Tank Conference, pp. 373–382.
- Zilman, G., March 2006. Forces exerted on a hovercraft by a moving pressure distribution: robustness of mathematical models. *J. Ship Res.* 50 (1), 38–48.